Egyptian Journal of Pure and Applied Science

Removal of ^{134}Cs(I) and ^{60}Co(II) from Radioactive Waste using Silver Nanoparticles

Alaa F. El-Daoushy[1*], Mohamed I. Aydia[1], Sami Elbayoumy[1], Wagiha H. Mahmoud[2], Tamer M. Sakr[1] and Khaled M. El-Azony[1]

[1] Radioactive isotopes and Generators Deptartment, Hot laboratories center, Egyptian Atomic Energy Authority, cairo, Egypt.

[2] Chemistry Deptartment., Faculty of Science, Ain shams University, cairo,Egypt

ARTICLE INFO

ABSTRACT

Silver metal nanoparticles were prepared and employed as an adsorbent for sorption of ^{134}Cs and ^{60}Co radionuclides. Batch equilibration technique was used to investigate the sorption behavior of ^{134}Cs and ^{60}Co radionuclides under different experimental parameters, such as the effect of pH, contact time, initial metal concentration (m_i), and temperature. The data showed that the sorption kinetics were best fitted to pseudo-second order model. Freundlich isotherm model was best fitted to the sorption of both ^{134}Cs and ^{60}Co radionuclides. Thermodynamic parameters ($\Delta H°$, $\Delta S°$, and $\Delta G°$) were calculated.

Introduction

In 2011, the huge power plant disaster at Fukushima Daiichi in Japan was the second most terrible atomic accident in the atomic power age history and had a staggering effect on the biological environment in the surrounding zone [1]. A Large measure of radioactive materials was discharged into the environment, because of which the surface water and soil particles were seriously contaminated. Among the released radionuclides, Cesium-134 (^{134}Cs) and Cesium-137 (^{137}Cs) radionuclides were detected and considered as hazardous radioisotopes due to their long half-lives [2]. Cesium can be effectively absorbed into earthborn and amphibian animals in view of its compound properties similar to that of potassium [3-5]. Accordingly, it can go into the human body and causes thyroid cancer through possibly irradiating in living tissues, liver, kidneys, and central nervous system causing psychological disorders [6].

^{60}Co radionuclide is produced in radioactive waste fluids by the activation of the non-radioactive cobalt(II) which is generated in the reactors from different metal surfaces and composites, for example, stellite (cobalt-chromium alloys designed for wear resistance) [7,8]. In addition, the irradiation of the inactive cobalt (II) in research reactors. Radioactive artificial isotope Co-60 is a beta producer that emits gamma radiation [9, 10]. Co-60 exposure causes loss of motion, looseness of the bowels, asthma, pneumonia, lung disturbances, weight reduction, vomiting, sickness, and harm to the thyroid and liver [11].

The removal of Cs-134 and Co-60 radionuclides from the radioactive wastewater is usually included with the few methodologies, for example, membrane filtration, evaporation, ion-exchange, solvent extraction, adsorption, and co-precipitation [5, 12, 13]. Utilization of the extensive amount of chemicals and the related expense, inefficient expulsion process, issues identified with the isolated radionuclide transfer are considered as the major disadvantages of these procedures [14,15]. For ion exchange process, the use of inorganic ion exchangers is commonly better than the organic ion exchangers in view of their thermal stability and the specific particle selectivity [16,17]. Adsorption is considered a promising technique for the removal of Cs-134 and Co-60 due to the efficient removal profile, ease of applicability, suitability for low contaminated wastewater, availability of many low-cost adsorbents [18]. Recently, nanomaterials have attracted much interest due to their unique characteristics differing from their bulk materials. They possess large sorption capacity, fast kinetics, high separation efficiency and reusability [19]. Within the past few years, nanomaterials have been under dynamic innovative work and have been effectively connected in numerous fields, for example, catalysis [20], detecting [21], prescription [22], and science [23]. Specifically, the use of nanomaterials in water and wastewater treatment has drawn wide consideration. This may be attributed to their small sizes resulting in large exposed surface areas, high adsorption capacity and reactivity. Furthermore, they possess high mobility in aqueous solutions [24]. It has been reported that nanomaterials showed superior removing ability of organic pollutants [25], bacteria [26], inorganic anions [27],

* Corresponding author.
 E-mail address: alaafeldaoushy_eaeae@yahoo.com

and heavy metals [28,29]. Based on various investigations, nanomaterials [30,31] show extraordinary guarantee for applications in water and wastewater treatment. Recently, the most broadly examined nanomaterials for water and wastewater treatment basically incorporate zero-valent metal nanoparticles, metal oxides nanoparticles, carbon nanotubes (CNTs), and nanocomposites.

In this work, we investigated the sorption efficiency of silver metal nanoparticles for removal performance of Cs-34 and Co-60 radionuclides under the different experimental conditions such as initial metal solution pH, contact time, initial metal concentration, and temperature in details. Moreover, adsorption kinetics, adsorption isotherm, and thermodynamics were also conducted to understand the adsorption behavior.

Subject and Methods

Chemicals

All chemicals used in this study were of analytical grade purity (A. R. grade), and they were used without further purification. Double distilled water was used for all solution preparations and washings. Silver nitrate ($AgNO_3$) was received from Winlab Co.-U.K., Cesium chloride (CsCl), cobalt chloride hexahydrate ($CoCl_2.6H_2O$), and sodium hydroxide were received from Sigma-Aldrich Co.-Germany. Nitric 37 % were received from Merk Co.-Germany.

Instrumentations

Radiometric identifications and measurements were performed by using a multichannel analyzer (MCA of "Inspector 2000" model, Canberra Series, made in U.S.A, coupled with a high-purity germanium coaxial detector (HPGe) of "GX2518" model. Samples of fixed geometry were counted with low dead time (< 5 %). A pH-meter with a microprocessor (Hanna Instruments pH211 model, Portugal) was used for measuring pH values of solutions. An analytical balance (A&D Engineering Inc., AND HR-202 model, USA) having dual range (42 g/0.01 mg, 210 g/0.1 mg) was used for weighing.

Radioactive isotopes

For radiochemical investigations, ^{60}Co (II) and ^{134}Cs (I) radionuclides were produced by thermal neutron irradiation of 100 mg of cobalt chloride and cesium chloride powders, respectively. The irradiation process was carried out in the 22 MW water-cooled Egyptian Second Research Reactor (ETRR-2) in Inshas, Egypt. Each target was wrapped in a thin aluminum foil, then placed in thick aluminum irradiation can, and irradiated at a thermal neutron flux of 10^{14} n.cm^{-2}.sec^{-1} for 4 hours. The radioactivity of $^{60}Co(II)$ and $^{134}Cs(I)$ radionuclides were radio-assayed using a multichannel analyzer. They could be detected from their characteristic peaks, (1173, 1332 keV) for ^{60}Co, and (605, 795 keV) for ^{134}Eu.

Method

Preparation of nano-silver metal

Silver nitrate ($AgNO_3$) and citric acid ($C_6H_8O_7$) were weighed and dissolved individually in minimum amount of distilled water. After that, the two solutions were mixed together with vigorous stirring and the resulting mixture was heated. The resulting powder of silver nanoparticles (AgNP) is then characterized using transmission electron microscopy (TEM) technique.

Batch mode adsorption studies

Batch equilibration technique was used to investigate the sorption behavior of Cs-134 and Co-60 radionuclides onto the prepared silver metal nano particles under different experimental parameters, such as the effect of pH, contact time, initial metal concentration (m_i), and temperature. This was achieved by adding 10 mL of 50 mg/L of ^{134}Cs or ^{60}Co radionuclides to equal amounts of silver metal nano-particles, and placing them in a thermostated water bath shaker at 25°C ±1 until achieving equilibrium, and then the supernatants were separated and applied for radiometric assay. The desired pH value was adjusted using hydrochloric acid or sodium hydroxide and measured before and after achieving equilibrium. Considering the effect of contact time, the development of removal percent was studied by varying the contact time from 15 to 480 minutes for ^{134}Cs radionuclide and from 15 to 2880 minutes for ^{60}Co radionuclide. The effect of temperature was performed at three different temperatures, 25 °C, 40 °C, 60 °C using concentrations of 100 mg/L and 200 mg/L. The removal percentage, R %, can be calculated using the following equation:

$$R \% = \frac{A_o - A_e}{A_o} * 100 \qquad (1)$$

Where A_o and A_e are the initial and final measured activity of the aqueous phase in counts/sec, respectively. Whereas the distribution coefficient, K_d, of the metal ions between liquid phase and solid phase, sorbent material, was determined using the following equation:

$$K_d = \frac{A_o - A_e}{A_e} * \frac{v}{m} \quad (mg/L) \qquad (2)$$

Where v is the volume (10 mL) of the aqueous solution and v is the sorbent weight (100 mg).

Results and discussion

Characterization

High resolution transmission electron microscopy **(HRTEM)** was carried out to confirm the formation of silver particles in the nano range. **Fig. 1** displays TEM image for the synthesized silver nanoparticles which reveals the formation of nanoparticles with average size less than 25 nm.

Effect of pH

The pH value of the liquid phase can be considered as the major influential parameter affecting the sorption process of metal ions [32]. The change in pH values affects the type and ionic state of the functional group existing on the solid phase surface in addition to affecting the ionization/dissociation of the adsorbate species [33]. Studying the effect of initial pH on the sorption of 50 mg/L of $^{134}Cs^+$ and $^{60}Co^{+2}$ radionuclides was carried out at room temperature The effect of initial pH onto removal percent of ^{134}Cs and ^{60}Co radionuclides and the relation between the initial and final pH values are shown in **Fig. 2**.

The uptake percent of both radionuclides increases gradually as the initial pH values increases. This can be attributed to the fact that at lower pH values there are an excess of H^+ ions competing with $^{134}Cs^+$ and $^{60}Co^{+2}$ radionuclides for sorption onto silver metal nanoparticles while with increasing the pH of the solution, the percent of H^+ ions decreases favoring the adsorption of those positively charged metal cations. These results are in good conformity with the literature reports [34].

Effect of contact time

Fig. 3 displays the effect of contact time on the removal

percent of $^{134}Cs^+$ and $^{60}Co^{+2}$ radionuclides. The removal percent increases with time till equilibrium is attained at 5.5 hours and 16 hours for ^{134}Cs and ^{60}Co, respectively. This may be attributed to the higher adsorbent surface area and accessibility of abundant active sites being available for the sorption of the ions onto the surface of prepared silver metal nanoparticles. At late contact time stages, the removal percent of ^{134}Cs and ^{60}Co radionuclides became relatively slow which may be explained by the obstruction of the sorption of more ions caused by those adsorbed at early stages [35].
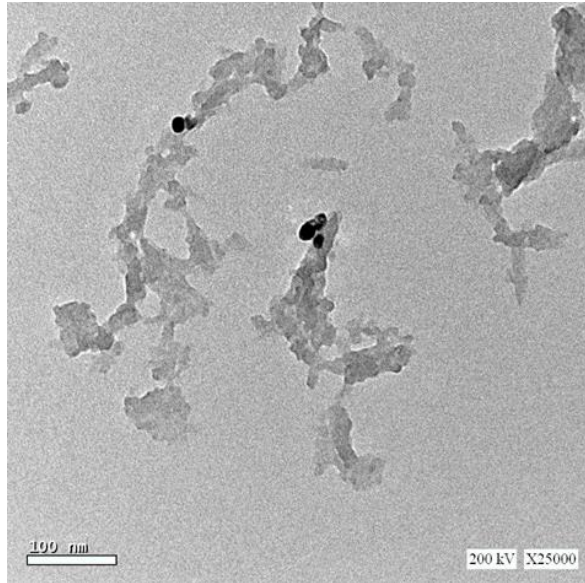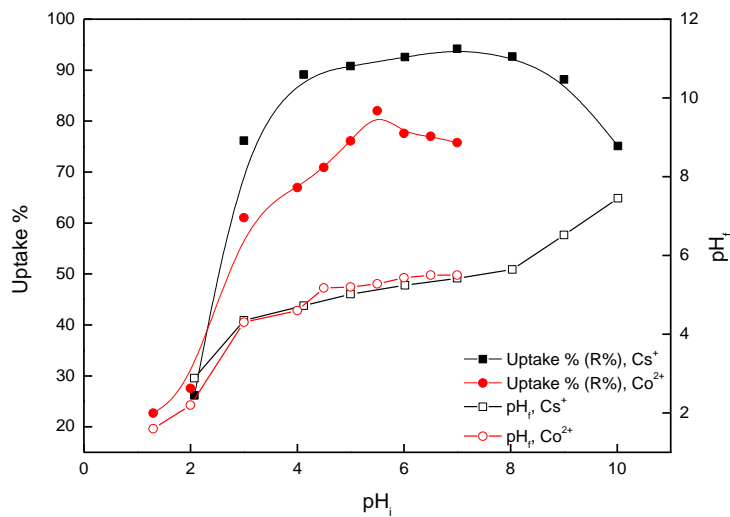

Fig.1: TEM image of synthesized silvr nanoparticles.

Fig. 2: Effect of initial and final pH on ^{134}Cs and ^{60}Co sorption onto prepared silver metal nanoparticles.
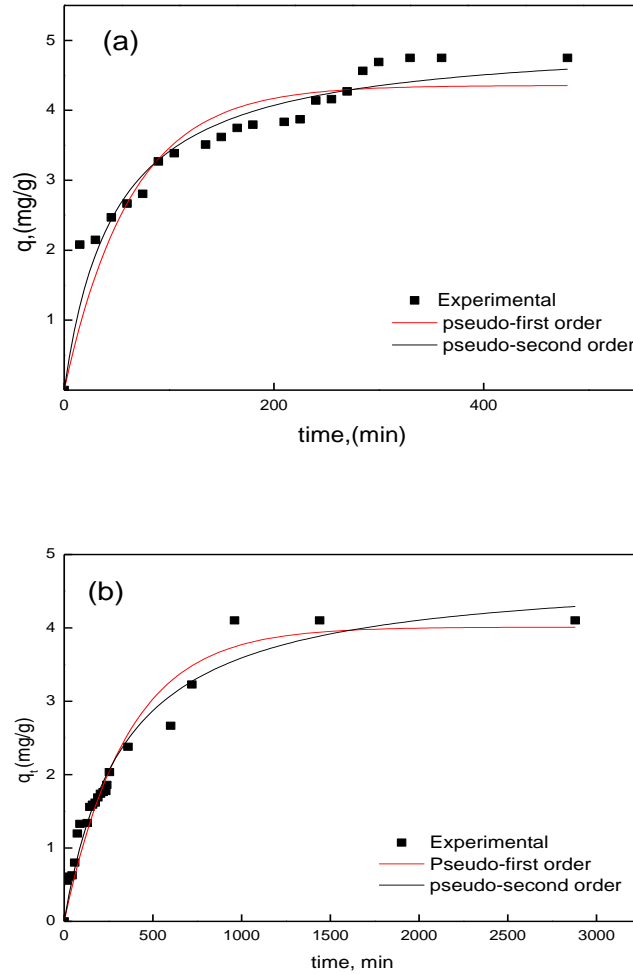
Fig.3: Effect of contact time and kinetic models for sorption of (a) [134]Cs and (b) ^{60}Co radionuclides onto silver metal nanoparticles.

Adsorption kinetics

The non-linear form of pseudo-first order rate expression of Lagergren model is expressed as follows [36]:

$$q_t = q_e(1 - exp^{-k_1 t})\qquad(3)$$

Where q_t and q_e are the amount of [134]Cs and ^{60}Co adsorbed in (mg/g) at time (t) and at equilibrium, respectively. k_1 is the lagergren rate constant of pseudo-first order in (min^{-1}).

The non-linear Pseudo-second order rate model equation can be expressed as follows [37]:

$$q_t = \frac{k_2 q_e^2 t}{1 + k_2 q_e t}\qquad(4)$$

Where q_t and q_e are the amount of [134]Cs and ^{60}Co adsorbed in (mg/g) at time (t) and at equilibrium, respectively. k_2 is the pseudo-second order rate constant in (g.mg^{-1} min^{-1}).

Fig. 3 shows the Effect of contact time and kinetic models for sorption of (a) 134Cs and (b) 60Co radionuclides onto silver metal nanoparticles. From **Table 1**, by comparing the values of the correlation coefficient (R2) of the sorption kinetic models for both 134Cs and ^{60}Co radionuclides, it can be deduced that the

sorption of [134]Cs and ^{60}Co radionuclides onto prepared radionuclides, it can be deduced that the sorption of [134]Cs and ^{60}Co radionuclides onto prepared silver metal nanoparticles is best fitted to pseudo-second order model.

Diffusion mechanism

In the current work, the three diffusion models were applied to predict the sorption mechanism of [134]Cs and ^{60}Co radionuclides onto silver metal nanoparticles.

The film diffusion model, proposed by McKay, can be represented by the following equation [38]:

$$\ln\left(\frac{1-q_t}{q_e}\right) = -k_f t\qquad(5)$$

Where q_t and q_e are the amount of [134]Cs and ^{60}Co adsorbed in (mg/g) at time (t) and at equilibrium, respectively. (t) is time in minutes, k_f is the rate constant for film diffusion in (min^{-1}). Film diffusion model can be obtained by plotting time (t) versus $\ln\left(\frac{1-q_t}{q_e}\right)$, where the value of k_f can be obtained from the slope.

The intraparticle diffusion model, proposed by Weber and Morris can be represented by the following equation [39]:

$$q_t = k_{ip} t^{1/2} + C\qquad(6)$$

Where q_t is amount of [134]Cs and ^{60}Co adsorbed in (mg/g) at time (t), k_{ip} is intraparticle diffusion rate constant in (mg/g min[1/2]), C is the intercept related to the thickness of boundary layer.

The pore diffusion model, proposed by Bangham, can be represented by Bangham's equation as follows [40]:

$$\log\left(log\left(\frac{C_i}{C_{i-}q_tw}\right)\right) = \log(\frac{k_bw}{2.303\,v}) + \sigma\log(t) \qquad (7)$$

Where C_i is initial metal concentration in aqueous phase, q_t is amount of [134]Cs and ^{60}Co adsorbed in (mg/g) at time (t), w is the weight of adsorbent material per liter of solution in (g/L), k_b and σ are Bangham's equation constants: $\sigma < 1$, v is the volume

of solution in (L). **Fig. 4 (a, b, c)** shows the film diffusion models, intraparticle diffusion models and pore diffusion models of both [134]Cs and ^{60}Co radionuclides; respectively. The obtained diffusion model parameters and correlation coefficients (R^2) values are listed in **Table 2**.

By comparing the correlation coefficient values of film diffusion model (0.76503 and 0.95873) and Intraparticle diffusion model (0.93641 and 0.97833) for [134]Cs and ^{60}Co radionuclides; respectively. It can be deduced that the diffusion of [134]Cs and ^{60}Co radionuclides through the silver metal nanoparticles occurs through Intraparticle diffusion mechanism which is more emphasized by the correlation coefficient value of pore diffusion model (0.96585 and 0.96126).

Table 1: kinetic parameters for sorption of [134]Cs and ^{60}Co radionuclides onto silver metal nanoparticles

sample	Pseudo-first order			Pseudo-second order		
	$q_{e,1}$ (mg/g)	K_1 (min^{-1})	R^2	$q_{e,2}$ (mg/g)	K_2 (g/mg. min)	R^2
Cs-134	4.35578	0.01582	0.88076	5.04787	0.00413	0.9373
Co-60	4.01094	0.00282	0.94813	4.78975	6.251E-4	0.9616

Table 2: Diffusion models parameters for sorption of [134]Cs and ^{60}Co radionuclides onto prepared silver metal nanoparticles

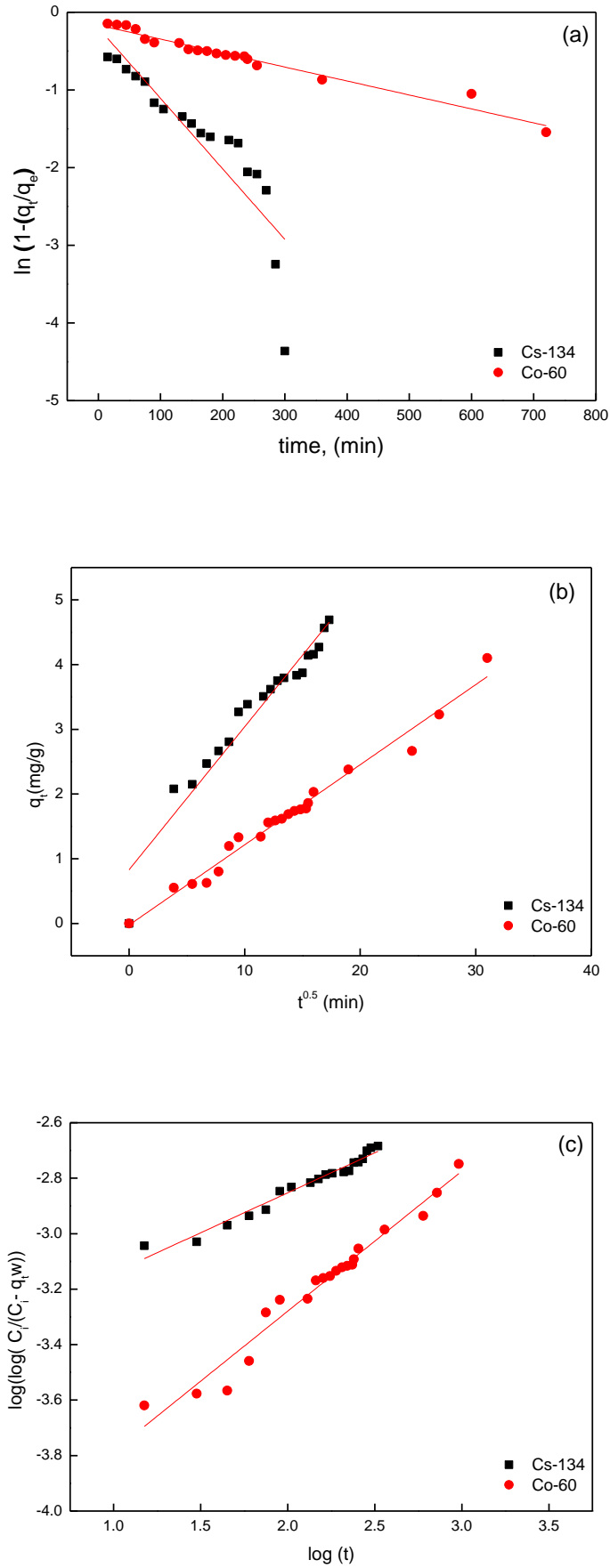| sample	Film Diffusion			Intraparticle Diffusion			Pore diffusion		
	slope $-k_f$ (min^{-1})	intercept	R^2	slope k_{ip} (mg/gmin[1/2])	intercept C	R^2	slope σ	intercept	R^2
Cs-134	-0.00908	-0.19995	0.76503	0.22099	0.82903	0.93641	0.28822	-3.42895	0.96585
Co-60	-0.0018	-0.16589	0.95873	0.12387	-0.0248	0.97833	0.5048	-4.28878	0.96126

Fig.4: Diffusion models for sorption of both ^{134}Cs and ^{60}Co radionuclides onto prepared silver metal nanoparticles (a) film diffusion, (b) intraparticle diffusion, and (c) pore diffusion.

Effect of initial metal concentration

The effect of initial concentration of ^{134}Cs and ^{60}Co radionuclides on their removal percent is shown in **Table 3.** It can be observed that, the removal percent decreases with increasing the initial metal concentration while the adsorbed amount of metal ions per unit mass of adsorbent increases. These results confirm that the adsorption process depends on the initial concentration of adsorbed ions. At low initial concentrations of metal ions, the number of the active sorption sites is much greater compared to the number of the metal ions present in the solution leading to higher removal percent. whereas at high metal ions concentrations, the available active sites are prone to larger number of metal ions which progressively fill up these sites interpreting the increase in the adsorbed amount of meta ions (q$_{eq}$) [41].

3.4.1 Adsorption isotherms

The non-linear form of Langmuir isotherm model can be expressed by the following equation:

$$q_e = \frac{q_m \, K_L \, C_e}{1 + K_L \, C_e} \qquad (8)$$

Where q_e is the adsorption capacity at equilibrium

(mg/g), q_m is the maximum monolayer coverage capacity in (mg/g), C_e is the equilibrium concentration of metal ion in (mg/L), and K_L is the Langmuir isotherm constant in (L/gm).

The non-linear regression of Freundlich isotherm model can be expressed by the following equation:

$$q_e = K_F \, C_e^{1/n} \qquad (9)$$

Where q_e is the adsorption capacity at equilibrium (mg/g) is, C_e is the equilibrium concentration of metal ion in (mg/L), K_F and n (measure of heterogeneity of of adsorption sites present on adsorbent surface) are Freundlich constants matching adsorption capacity and intensity; respectively.

Fig. 5 (a and b) shows the sorption isotherm models. The sorption isotherm parameters corresponding to the afore mentioned models are listed in **Table 4.** By comparing the values of the obtained correlation coefficients (R^2) for both ^{134}Cs and ^{60}Co radionuclides, it can be deduced that sorption process is best fitted to Freundlich isotherm model. The values of sorption intensity (n) (2.81341, 1.71513) for ^{134}Cs and ^{60}Co radionuclides; respectively, is greater than one indicating a favorable sorption process.

Table 3: Effect of initial metal concentration on both sorption capacity and removal percent of prepared silver metal nanoparticles

C_o (mg/L)		C_e (mg/L)		q_{eq} (mg/g)		R%	
Cs-134	**Co-60**	**Cs-134**	**Co-60**	**Cs-134**	**Co-60**	**Cs-134**	**Co-60**
10	50	0.5675	8.99163	0.9432	4.1008	94.32	82.01
20	100	0.44487	53.31266	1.9555	4.6687	97.77	46.68
50	200	1.75947	143.28652	4.8240	5.6713	96.45	28.35
75	300	5.11824	227.75	6.9881	7.225	93.17	24.08
100	589.33194	7.10247	499.51209	9.2897	8.9819	92.89	15.24
150	1178.6639	18.96131	1003.2714	13.1038	17.5392	87.35	14.88
200	1767.9958	40.40699	1507.7378	15.9593	26.0257	79.79	14.72
300	2946.6597	87.01888	2639.79418	21.2981	30.68	70.99	10.41
1329.05		915.36822		41.3681		31.12	
1993		1462.862		53.0138		26.6	
5316.2		4507.70899		80.8491		15.2	

Table 4: Sorption isotherm models' parameters for sorption of 134Cs and 60Co radionuclides onto prepared silver metal nanoparticles

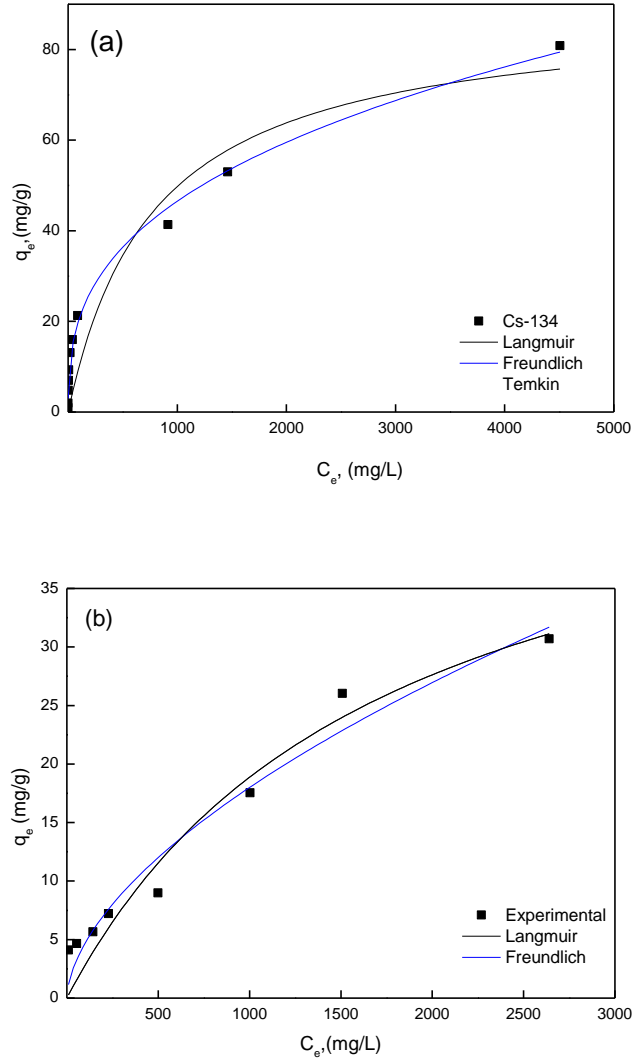| sample	Langmuir			Freundlich		
	q_{max} (mg/g)	K_L (L/gm)	R^2	K_F (mg^{1-n}L^n/g)	n	R^2
Cs-134	88.88	0.001272	0.88933	3.99311	2.81341	0.99461
Co-60	51.52	5.77742	0.93543	0.32061	1.71513	0.95173

Fig. 5: Effect of initial metal concentration and isotherm models for sorption of (a) [134]Cs and (b) ^{60}Co radionuclides onto prepared silver metal nanoparticles.

Effect of temperature and thermodynamic parameters

The effect of temperature is an important criterion for understanding the nature of the sorption process. Vant` Hoff equation was applied to determine the thermodynamic parameters such as; Gibbs free energy (ΔG^o), entropy change (ΔS^o), and enthalpy change (ΔH^o) as follows:

$$\ln K_d = (-\frac{\Delta H^o}{RT}) + (\frac{\Delta S^o}{R}) \qquad (10)$$

$$\Delta G^o = \Delta H^o - T\,\Delta S^o \qquad (11)$$

$$\Delta G^o = -R\,T \ln K_d \qquad (12)$$

Where K_d is the distribution coefficient in (mL/g), R is the general gas constant T is the kelvin temperature.

Fig. 6 shows the Arrhenius plot for the sorption of [134]Cs and ^{60}Co radionuclides onto the silver metal nanoparticles, and the thermodynamic parameters are listed in **Table 5**. For [134]Cs, it can be noted that the uptake percent decreases with increasing temperature indicating an exothermic process, which is further emphasized by the negative value of calculated enthalpy (ΔH^o). While in case of ^{60}Co, a remarkable increase in the uptake percent is noticed with increasing temperature implying the endothermic nature of sorption process, which was further proved by the positive value of calculated enthalpy (ΔH^o). This increase in uptake percent may be due to promoting the movement of metal ions from the aqueous phase to the surface of sorbent material and better contacting with the available active sites or it might be due to origination of new active sites [42]. For both [134]Cs and ^{60}Co radionuclides, the positive entropy (ΔS^o) value implies the spontaneity of the sorption process which is also further proved by the negative values of (ΔG^o), and the progressive increase in (ΔG^o) values with raising temperature indicates that the sorption process is less effective at higher temperatures.
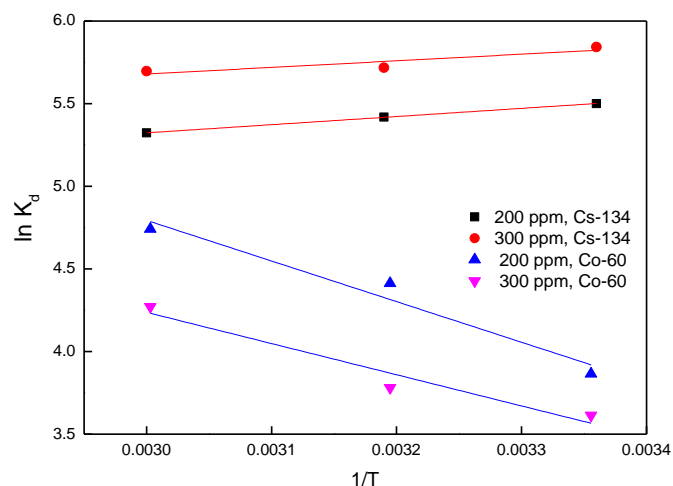
Fig. 6: Effect of reaction temperature on the sorption of ^{134}Cs and ^{60}Co radionuclides onto prepared silver metal nanoparticle.

Table 5: Thermodynamic parameters concerning sorption of ^{134}Cs and ^{60}Co radionuclides onto prepared silver metal nanoparticles

sample	Conc (mg/L)	slope	intercept	ΔH° (KJ.mol^{-1})	ΔS° (KJ.mol^{-1}.K^{-1})	ΔG° (KJ.mol^{-1})		
						298°K	313 °K	333 °K
Cs-134	200	493.60534	3.84267	-4.104268	0.031951967	-13.62595	-14.105234	-14.744273
	300	399.84687	4.47991	-3.3247113	0.037250535	-14.42537	-14.984129	-15.729139
Co-60	200	- 2458.90899	12.17049	20.44582	0.101197624	-9.711063	-11.229028	-13.252981
	300	- 1887.23077	9.89864	15.69232	0.082307192	-8.835219	-10.069827	-11.715971

Conclusion

Sorption of ^{134}Cs and ^{60}Co radionuclides onto the prepared silver metal nanoparticles are studied and the obtained results showed that the sorption process either of ^{134}Cs and ^{60}Co radionuclides is dependent on the pH value, adsorbate concentration, as well as the reaction temperature. The sorption process follows the pseudo-second order rate model. Freundlich isotherm model best describes the sorption behavior of both radionuclides. Thermodynamic studies indicate that the sorption of ^{134}Cs is an exothermic process, while that of ^{60}Co is endothermic.

References

1) **Khandakera, S., Toyohara Y., Kamida S. and Kuba T. (2018).** Adsorptive removal of cesium from aqueous solution using oxidized bamboo charcoal. Water Resources and Industry, **19:** 35–46. https://doi.org/10.1016/j.wri.2018.01.001

2) **Abtahi, M., Fakhri, Y., Sarafraz, M., Keramati, H., Conti, G. O., Ferrante, M., Nazak, A., Rokhsane, H. P., Bigard, M. and Zahra B. (2018).** Removal of cesium through adsorption from aqueous solutions:a systematic review. J. Adv. Environ. Health Res., **6**(2): 96-106. doi:10.22102/jaehr.2018.104959.1048.

3) **Nilchi, A., Saberi, R., Moradi, M., Azizpour, H. and Zarghami, R. (2011).** Adsorption of cesium on copper hexacyanoferrate-PAN composite ion exchanger from aqueous solution. Chem. Eng. J., **172:** 572–580. http://dx.doi.org/10.1016/j.cej.2011.06.011.

4) **Cortés-Martínez, R., Olguín, M. T. and Solache-Ríos, M. (2010).** Cesium sorption by clinoptilolite-rich tuffs in batch and fixed-bed systems. Desalination, **258:** 164–170, http://dx.doi.org/10.1016/j.desal.2010.03.019.

5) **Awual, M. R., Suzuki, S., Taguchi, T., Shiwaku, H., Okamoto, Y. and Yaita T. (2014).** Radioactive cesium removal from nuclear wastewater by novel inorganic and conjugate adsorbents. Chem. Eng. J., **242:** 127–135, http://dx.doi.org/10.1016/j.cej.2013.12.072

6) **Sangvanich, T., Sukwarotwat, V., Wiacek, R. J., Grudzien, R. M., Fryxell, G. E., Addleman, R. S., Timchalk, C. and Yantasee W. (2010).** Selective capture of cesium and thallium from natural waters and simulated wastes with copper ferrocyanide functionalized mesoporous silica. J. Hazard. Mater., **182:** 225–231. http://dx.doi.org/ 10.1016/j.jhazmat.2010.06.019.

7) **Abdul Nishad, P., Bhaskarapillai, A., Velmurugan, S. and Narasimhan S. V. (2012).** Cobalt (II) imprinted chitosan for selective removal of cobalt during nuclear reactor decontamination. Carbohydr. Polym., **87:** 2690–2696.https://doi.org/10.1016/j.carbpol.2011.11.061.

8) **IAEA, (1981).** Decontamination of operational nuclear power plants, Vienna, AEATECDOC-**248,** https://inis.iaea.org/collection/ NCLCollectionStore/_Public/13/680/13680247.pdf.

9) **Park, Y., Shin, W. S. and Choi, S. J. (2013).** Removal of cobalt and strontium from groundwater by sorption onto fishbone J. Radioanal. Nucl. Chem., **295:** 789–799. DOI 10.1007/s10967-012-1959-8.

10) **Tizro, S. and Baseri, H. (2017).** Removal of Cobalt Ions from Contaminated Water Using Magnetite Based Nanocomposites: Effects of Various Parameters on the Removal Efficiency. J. Water Environ. Nanotechnol., **2**(3): 174-185. DOI: 10.22090/ jwent.2017.03.005

11) **Sobhanardakani, S. and Zandipak, R. (2015).** Adsorption of Co (II) ions from aqueous solutions using NiFe2O4 nanoparticles. J. Adv. Environ. Health Res., **3**(3): 179-87.

12) **Tsai, S. C., Wang, T. H., Li, M. H., Wei, Y. Y. and Teng, S. P. (2009).** Cesium adsorption and distribution onto crushed granite under different physicochemical conditions. J. Hazard. Mater., **161:** 854–861, http://dx.doi.org/10.1016/j.jhazmat.2008.04.044.

13) **Chen, R., Tanaka, H., Kawamoto, T., Asai, M., Fukushima, C., Na, H., Kurihara, M., Watanabe, M., Arisaka, M. and Nankawa T. (2013).** Selective removal of cesium ions from wastewater using copper hexacyanoferrate nanofilms in an electrochemical system. Electrochim. Acta., **87:** 119–125. http://dx.doi.org/10.1016/j. electacta.2012.08.124.

14) **Pangeni, B., Paudyal, H., Inoue, K., Ohto, K., Kawakita, H. and Alam, S. (2014).** Preparation of natural cation exchanger from persimmon waste and its application for the removal of cesium from water. Chem. Eng. J., **242:** 109–116. http://dx.doi.org/10.1016/j.cej.2013.12.042.

15) **Ding, D., Zhao, Y., Yang, S., Shi, W., Zhang, Z., Lei, Z. and Yang Y. (2013).** Adsorption of cesium from aqueous solution using agricultural residue - Walnut shell: equilibrium, kinetic and thermodynamic modeling studies. Water Res., **47** 2563–2571, http://dx.doi.org/10.1016/j.watres.2013.02.014.

16) **Awual, M. R., Miyazaki, Y., Taguchi, T., Shiwaku H. and Yaita T. (2016).** Encapsulation of cesium from contaminated water with highly selective facial organic-inorganic mesoporous hybrid adsorbent. Chem. Eng. J., **291:** 128–137. http://dx.doi.org/10.1016/j.cej.2016.01.109.

17) **Yang, H., Yu, H., Sun ,J., Liu, J., Xia, J., Fang, J., Li, Y., Qu, F., Song, A. and Wu, T. (2017).** Facile synthesis of mesoporous magnetic AMP polyhedric composites for rapid and highly efficient separation of Cs+ from water. Chem. Eng. J., **317:** 533–543. http://dx.doi.org/10.1016/j.cej.2017.02.088.

18) **Ishihara, R., Fujiwara, K., Harayama, T., Okamura, Y., Uchiyama, S., Sugiyama, M., Someya, T., Amakai, W., Umino, S., Ono, T., Nide, A., Hirayama, Y., Baba, T., Kojima, T., Umeno, D., Saito, K., Asai, S. and Sugo T. (2011).** Removal of cesium using cobalt-ferrocyanide-impregnated polymer-chain-grafted fibers. J. Nucl. Sci. Technol., **48:** 1281–1284, http://dx.doi.org/10.1080/18811248.2011.9711817

19) **Lu, H., Wang, J., Stoller, M., Wang, T., Bao, Y. and Hao, H. (2016).** An Overview of Nanomaterials for Water and Wastewater Treatment, a review article. Advances in Materials Science and Engineering, http://dx.doi.org/10.1155/2016/4964828

20) **Parmon, V. (2008).** Nanomaterials in catalysis. Materials Research Innovations, **12**(2): 60–61

21) **Kusior, A., Klich-Kafel, J., Trenczek-Zajac, A., Swierczek, K., Radecka, M. and Zakrzewska, K. (2013).** TiO2–SnO2 nanomaterials for gas sensing and photocatalysis. Journal of the European Ceramic Society, **33**(12): 2285–2290.

22) **Liang, X. J., Kumar, A., Shi, D. and Cui, D. (2012).** Nanostructures for medicine and pharmaceuticals. Journal of Nanomaterials, Article ID 921897.

23) **Bujoli, B., Roussière, H., Montavon, G., Laïb,S., Janvier, P., Alonso, B., Fayon, F., Petit, M., Massiot, D., Bouler, J., Guicheux, J., Gauthier, O., Lane, S. M., Nonglaton, G., Pipelier, M., Léger, J., Talham, D, R. and Tellier, C. (2006).** Novel phosphate–phosphonate hybrid nanomaterials applied to biology. Progress in Solid State Chemistry, **34**(2–4): 257–266.

24) **Khin, M. M., Nair, A. S., Babu, V. J., Murugan, R. and Ramakrishna, S. (2012).** A review on nanomaterials for environmental remediation. Energy & Environmental Science, **5**(8): 8075–8109.

25) **Yan, J., Han, L., Gao, W., Xue, S. and Chen, M. (2015).** Biochar supported nanoscale zerovalent iron composite used as persulfate activator for removing trichloroethylene. Bioresource Technology, **175:** 269–274.

26) **Liu, F., Yang, J. H., Zuo, J., Ma, D., Gan, L., Xie, B., Wang, P. and Yang. B. (2014):** Graphene-supported nanoscale zero-valent iron: removal of phosphorus from aqueous solution and mechanistic study. Journal of Environmental Sciences, **26**(8): 1751–1762.

27) **Kalhapure, R. S., Sonawane, S. J., Sikwal, D. R., Jadhav, M., Eambharose, S., Mocktar, C. and Govender, T. (2015):** Solid lipid nanoparticles of clotrimazole silver complex: an efficient nano antibacterial against *Staphylococcus aureus* and MRSA. Colloids and Surfaces B: Biointerfaces, **136:** 51–658.

28) **Hashemzadeh, M., Nilchi, A., Hassani, A. H. and Saberi, R. (2018).** Synthesis of novel surface-modified hematite nanoparticles for the removal of cobalt-60 radiocations from aqueous solution. International Journal of Environmental Science and Technology, **16:** 775-792. https://doi.org/10.1007/s13762-018-1656-4.

29) **Kim, Y., Kim, I., Lee, T. S., Lee, E. and Lee, K. J. (2017).** Porous hydrogel containing Prussian blue nanoparticles for effective cesium ion adsorption in aqueous media. Journal of Industrisl and Engineering Chemistry, 60: 465-474. https://doi.org/10.1016/j.jiec.2017.11.034.

30) **Shabnam, T., Seiyed, M. H. and Behzad, A. (2019).** Engineering nanomaterials for water and wastewater treatment: review of classifications, properties and applications. NJC., **43**(21): 7902-7927.

31) **Michał, B., Krystyna, K. and Anna, K. (2019).** Nanotechnology in water and wastewater treatment. Graphene – the nanomaterial for next generation of semipermeable membranes. Critical Reviews in Environmental Science and Technology, DOI: 10.1080/10643389.2019.1664258.

32) **Gupta, V. K., Agarwal, S. and Saleh, T. A. (2011).** Synthesis and characterization of alumina-coated carbon nanotubes and their application for lead removal. J. Hazard. Mater., **185:** 17–23.

33) **Rizk, S. E. and Hamed, M. M. (2015).** Batch sorption of iron complex dye, naphthol green B, from wastewater on charcoal, kaolinite, and tafla. Desalination and Water Treatment, **56** (6):1536–46, d moi:10.1080/19443994.2014.954004.

34) **Hamed, M. M., Aly, M. I. and Nayl, A. A. (2016).** Kinetics and thermodynamics studies of cobalt, strontium and cesium sorption on marble from aqueous solution. Chemistry and Ecology, **32** (1):68–87, doi:10.1080/02757540.2015.1112379.

35) **Yao, W., Yu, S., Wang, J., Zou, Y., Lu, S., Ai, Y., Alharbi, S. N., Alsaedi, A., Hayat, T. and Wang X. (2017).** Enhanced removal of methyl orange on calcined glycerol-modified nanocrystallined Mg/Al layered double hydroxides. Chem. Eng. J., **307:** 476–486. https://doi.org/10.1016/j.cej.2016. 08.117.

36) **Lagergren, S. (1898).** About the theory of so-called adsorption of soluble substances. Kungl Svenska vetenskapsakademiens handlingar, **241:** 1–39.

37) **Largitte, L. and Pasquier, R. (2016).** A review of the kinetics adsorption models and their application to the adsorption of lead by an activated carbon. chemical engineering research and design, **109:** 495–504, http://dx.doi.org/10.1016/j.cherd.2016.02.006.

38) **McKay, G. and Poots, V. J. P. (1980).** Kinetics and diffusion processes in colour removal from effluent using wood as an adsorbent. J. Chem. Technol. Biotechnol., **30**(1): 279-292. https://doi.org/10.1002/jctb.503300134.

39) **Weber, W. J. and Morris J. C. (1963).** Kinetics of Adsorption on Carbon from Solution. Journal of the Sanitary Engineering Division, **89**(2): 31–60.

40) **Singh, T. P. and Majumder, C. B. (2015).** Kinetics for Removal of Fluoride from Aqueous Solution Through Adsorption From Mousambi Peel, Ground Nut Shell and Neem Leaves. International Journal of Science, Engineering and Technology, **3**(4): 879-883.

41) **Vieira, M. G. A., Neto, A. F. A., Gimenes, M. L. and Silva, M. G. C. (2010).** Sorption kinetics and equilibrium for the removal of nickel ions from aqueous phase on calcined Bofe bentonite clay. Journal of Hazardous Materials, **177:** 362–371.

42) **Dada, A. O., Olalekan, A. P., Olatunya, A. M. and DADA, O. (2012).** Langmuir, Freundlich, Temkin and Dubinin–Radushkevich Isotherms Studies of Equilibrium Sorption of Zn^{2+} Unto Phosphoric Acid Modified Rice Husk. Journal of Applied Chemistry, **3**(1): 38-45.